THE JOURNAL OF PHYSICAL CHEMISTRY C
A JOURNAL OF THE AMERICAN CHEMICAL SOCIETY

Open Access
This article is licensed under CC-BY-NC-ND 4.0

In Situ Tracking of Pt Migration from Pt/Al_2O_3 to CeO_2 on the Atomic and Reactor Scale

Samuel Struzek, Birger Holtermann, Shweta Sharma, Florian Maurer, Jelena Jelic, Anna Zimina, Felix Studt, Yolita M. Eggeler,* and Jan-Dierk Grunwaldt*

Cite This: https://doi.org/10.1021/acs.jpcc.5c05574 **Read Online**

ACCESS | Metrics & More | Article Recommendations | Supporting Information

ABSTRACT: Pt through the gas phase in the form of volatile PtO_2 has become a topic of interest within recent years due to its application in the production of single atom catalysts. It is furthermore important for oxidation reactions that take place at high temperatures, e.g., CH_4 oxidation in order to track noble metal loss. Here, platinum migration is observed on the nanometer scale for mixed Pt/Al_2O_3 and CeO_2 nanoparticles as grinded powders. Furthermore, Pt migration within a reactor in a dual bed of Pt/Al_2O_3 followed by a bed of sieved CeO_2 particles is tracked *in situ* on the millimeter scale *via* time and spatially resolved X-ray absorption spectroscopy. It is observed that gaseous PtO_2 is first captured at the beginning of the CeO_2 bed. When the beginning of the bed appears saturated, PtO_2 adsorbs further downstream. Such adsorption behavior has to our knowledge not yet been reported in the literature since it requires time and spatially resolved *in situ* tracking. Furthermore, preferential adsorption sites of Pt on CeO_2 were identified using experimental extended X-ray absorption fine structure data and fitting based on models from Density Functional Theory calculations. They point to geometries as, for example, found in 4-fold hollow sites on CeO_2 (110) with additional ligands for stabilization.

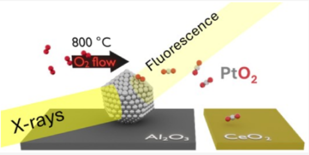

INTRODUCTION

Platinum (Pt) deposited on support materials like Al_2O_3 or CeO_2 is often utilized for emission control purposes.[1−4] Metallic Pt atoms are immobile on support materials at operation temperatures relevant for catalysis (<1000 °C) due to the high sublimation energy of Pt and the high energy barrier for single atom detachment (both energies are >500 kJ/mol).[5] This picture changes under oxidative conditions since for temperatures as low as 450 °C[6,7] oxidized Pt is known to become volatile in the form of PtO_2 entities.[8,9] At 800 °C, it has been shown that almost all of the Pt is lost within a timespan of hours.[10] Volatile PtO_2 is capable of migrating either onto the support material or into the gas phase.[11] This poses a major challenge to the performance stability of catalysts that operate at high temperatures as the migration leads to Pt sintering and potentially even to a loss of the active and costly precious metal. Examples in this regard are 3-way and diesel oxidation catalysts within the automotive industry, as well as industrial flue gas after treatment catalysts.[12,13] Furthermore, the volatility of Pt is also relevant within other fields of research, e.g., in solid oxide fuel cells (SOFCs).[14,15] In order to prevent the gas phase migration of PtO_2, Knudsen diffusion inside nm-sized pores can be utilized.[16] However, the gas phase migration is not always undesirable since it offers unique possibilities for the preparation of functional nanomaterials as shown by Datye et al.[17,18] for the formation of Pt−Pd alloys or its migration from Al_2O_3 to CeO_2 for the formation of Pt single atom catalysts.[19] Surface doping of CeO_2 was shown to stabilize the CeO_2 surface area during calcination in air at 800 °C.[20] This could be another area in which Pt migration could be used. In regard to the trapping mechanism, Bruix et al. claimed that CeO_2 nanopockets on (100) nanofacets next to defect sites on the CeO_2 surface are the most preferential sites for Pt incorporation.[21,22] Jones et al. revealed that CeO_2 rods and cubes, known to exhibit mostly (100) and (111) facets,[23] change at 800 °C in air toward more rounded shapes, which contain more sites for Pt adsorption.[19] Maurer et al. discovered that under oxidative conditions above 600 °C, Pt atoms become incorporated onto CeO_2 in (110) nanopockets, which start to form under these conditions.[24] Even though there has been a lot of research conducted within the topic of Pt sintering and its migration and deposition onto CeO_2, there are still open questions in regard to *in situ* and *operando* tracking, the length scale for the migration, and preferential deposition sites of Pt, which are tackled within this work. In a first step, Pt migration is shown to occur on length scales of ∼nm to μm by mixing Pt/Al_2O_3 with CeO_2 using electron microscopy (EM) and catalytic studies. In a second step, *in situ* live tracking of the Pt migration is conducted on a mm length scale in a time and spatially resolved manner *via* X-ray absorption spectroscopy (XAS). To this end, a spatially separated Pt/Al_2O_3 and CeO_2 packed powder bed is utilized. Finally, the preferential Pt adsorption sites on CeO_2 are

Received: August 8, 2025
Revised: January 9, 2026
Accepted: January 14, 2026

Downloaded via KIT BIBLIOTHEK on February 16, 2026 at 08:42:54 (UTC).
See https://pubs.acs.org/sharingguidelines for options on how to legitimately share published articles.

ACS Publications
© XXXX The Authors. Published by American Chemical Society

identified by EXAFS fitting using various density functional theory (DFT)-derived structures.

■ EXPERIMENTAL AND METHODS

Catalyst Preparation

Pt/Al_2O_3 and Pt/CeO_2 catalysts were prepared by automated incipient wetness impregnation using a SYNTHESIZER CATIMPREG platform by Chemspeed Technologies AG, utilizing tetraamine platinum nitrate (Alfa Aesar) as the precursor. As supports, commercially available γ-alumina (Puralox TH 100/150, Sasol Germany GmbH) and CeO_2 (HSA 20, Solvay) were used. The CeO_2 average crystalline domain size after 5 h of calcination at 700 °C was 8.6 nm (see SI) and its specific surface area 104 $\frac{m^2}{g}$. The Pt/Al_2O_3 catalyst exhibited an average Pt particle size of 2.0 ± 0.9 nm and a Pt loading of 1.9 ± 0.1 wt %. The Pt/CeO_2 catalyst exhibited an average Pt particle size of 1.0 ± 0.30 nm and a Pt loading of 1.91 ± 0.10 wt %. Particle sizes were determined *via* transmission electron microscopy (TEM). The Pt loading was determined by inductively coupled plasma optical emission spectroscopy (ICP-OES). For *in situ* and *operando* measurements, CeO_2 and Pt/Al_2O_3 packed powder beds with the sieve fraction of 100−200 μm were used. The Pt/CeO_2 catalyst was utilized only for calibration purposes but not within the experiments.

Pt Migration from Pt/Al_2O_3 to Adjacent CeO_2

1.9 wt % Pt/Al_2O_3 and CeO_2 powders were mixed in a ratio of 1:1 and calcined for 12 h at either 400 °C or 800 °C in static air inside a furnace (without sieving). Part of the powders was taken aside after calcination for high-angle annular dark-field scanning transmission electron microscopy (HAADF-STEM) and energy-dispersive X-ray spectroscopy (EDX) investigations (Device: FEI Tecnai Osiris; Detector: Super-X Quad Silicon Drift Detector). Due to the similar contrast of Pt and CeO_2 in HAADF-STEM, an additional pretreatment step in 5% H_2/N_2 at 400 °C was carried out beforehand for 1 h. This was done to ensure the formation of Pt clusters and particles, so they can be better resolved on CeO_2.

In addition, Pt migration of a single Pt/Al_2O_3 particle was studied on the μm scale using a microelectromechanical system (MEMS)-based transmission electron microscopy (TEM) chip. For further details, see Chapter "*In situ* fluorescence study of a Pt/Al_2O_3 particle" in the SI.

Catalytic CO and NO Oxidation Activity

After 12 h of calcination, the 1:1 mixed 1.9 wt % Pt/Al_2O_3 + CeO_2 powders were pressed, sieved (100−200 μm), and put inside quartz microreactors with an inner diameter of 8 mm (1 mm wall thickness), where the powders were held in place by quartz wool. Each powder bed contained 100 mg of the catalyst. The temperature in the reactor was continuously monitored using two thermocouples placed upstream and downstream of the catalyst bed. The upstream thermocouple was also used to control the furnace. Gases (CO, NO, O_2, N_2) were dosed by mass-flow controllers (MFC, Bronkhorst Deutschland Nord GmbH), and the gas composition was measured behind the reactor outlet by a Fourier transform infrared (FTIR) spectrometer (Multigas 2030, MKS Instruments). The applied gas flow was 1 $\frac{l}{min}$, containing 10% O_2, 1000 ppm of either CO or NO and N_2 with a weight hourly space velocity (WHSV) of 6.4×10^4 $\frac{l}{hg}$ (liters of all gases combined per hour and grams of Pt).

In Situ XAS during the Pt Migration from Al_2O_3 to Spatially Separated CeO_2 and *Operando* CO Oxidation Tests

The *in situ* XAS measurements during the Pt migration from Al_2O_3 to spatially separated CeO_2 and *operando* XAS measurements during the catalytic CO oxidation tests were conducted at the P65 beamline (DESY synchrotron, Hamburg).[25] X-rays were generated by an 11 period undulator. Harmonics were removed *via* two water-cooled Si-coated plane mirrors, installed before a Si(111) double crystal monochromator (DCM). The photon flux at the sample was between 10^{11} and 10^{12} $\frac{1}{s}$ with a relative bandwidth of 10^{-4}. Measurements were conducted at the Pt L3-edge (11564 eV) with a measuring time of 3 min per spectra during light-off experiments and 6 min during the migration experiments. XAS data were treated and evaluated using the Athena software.[26] Hereby, the pre-edge normalization was conducted from −175 to −90 eV with respect to the absorption edge and the postedge normalization from 100 to 980 eV with a normalization order of 3. Linear combination analysis (LCA) was performed using an oxidized and a reduced Pt/Al_2O_3 sample as reference. Figure 1 displays the experimental setup at the beamline. Gases were dosed by mass-flow controllers (MFC, Bronkhorst Deutschland Nord GmbH) through a quartz microreactor (outer diameter = 1.5 mm, 0.01 mm wall thickness). The catalyst inside the reactor was heated by a hot-air blower (FMB Oxford) that was placed below the reactor. An infrared (IR) camera (ImageIR, InfraTec GmbH) recorded the temperature of the catalyst. The incoming X-ray beam was directed at 45° to the gas flow direction along the catalyst within the reactor, and the fluorescence signal was collected at 90° relative to the incoming beam by an energy dispersive 4 pixel SDD detector. The gas flow was analyzed behind the reactor outlet by a FTIR spectrometer (Multigas 2030, MKS Instruments). To increase the time resolution of the spectrometer, the product flow from the reactor was diluted by inert gas in a ratio of 1:4. Figure 1b shows the catalysts within the quartz microreactor. A Pt/Al_2O_3 (upstream) and a second CeO_2 catalyst bed (downstream) were placed within the microreactor, held in place, and separated by quartz wool. Figure 1c displays the temperature distributions of the Pt/Al_2O_3 and the CeO_2 packed beds during the Pt migration (50 $\frac{ml}{min}$ gas flow, containing 10% O_2 in He). The catalyst packed beds contained 1.9 mg of 1.9 wt % Pt/Al_2O_3 and 4.4 mg of CeO_2 in order to obtain two packed powder beds similar in length. The resulting WHSV was 8×10^4 $\frac{l}{hg}$. For the CO oxidation experiments, performed before and after the Pt migration on the very same catalyst, the gas flow and WHSV were identical, and the gas composition was 10% O_2, 1000 ppm of CO, and He.

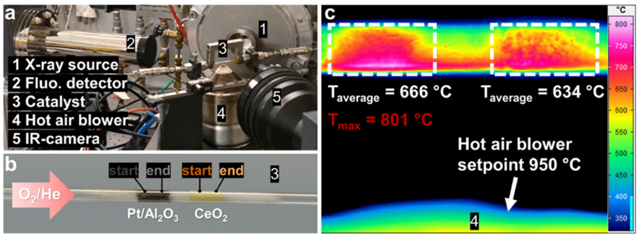

Figure 1. (a) *In situ/operando* XAS setup at the P65 beamline. The catalyst within the capillary reactor was located at position 3. (b) 1.9 wt % Pt/Al_2O_3 catalyst powder bed (gray) and CeO_2 powder bed (yellow) inside a quartz microreactor, separated by quartz wool. The gas flow was directed from left to right. Four measurement positions for the X-ray beam (start and end, respectively) are indicated (beam size $H \times W$ = 0.3 mm × 0.5 mm). (c) IR thermography image of the Pt/Al_2O_3 (left) and CeO_2 (right) packed powder beds during the gas phase migration experiment in 10% O_2/He.

In Situ Quantification of the Pt Loading

The amount of Pt on Al_2O_3 and CeO_2 was obtained *via* XAS in fluorescence mode. Figure 2a depicts the Pt L3-edge fluorescence X-ray absorption near edge structure (XANES) of a quartz reactor with 1.5 mm diameter, filled with a reference powder containing 0.94 wt % Pt/Al_2O_3 of a 100−200 μm sieve fraction. The edge-step, which is the jump in the total X-ray absorption μ(E) at the L3-transition energy of 11564 eV from the baseline of the pre-edge to that of the postedge (both depicted as blue dashed lines in Figure 2), was 1.6 for this specific Pt loading. The pre-edge (−175 to −90 eV) and the postedge (100 to 980 eV with respect to the absorption edge, normalization

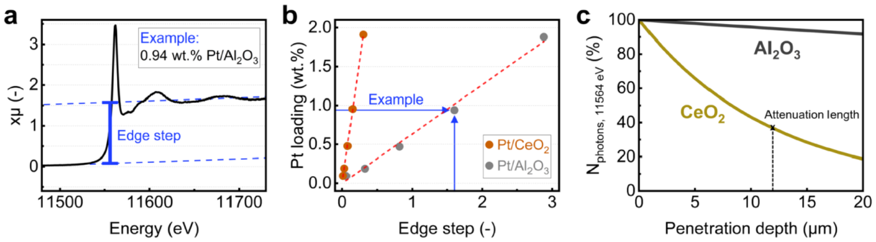

Figure 2. Method for tracking Pt loading by XAS. (a) Exemplary Pt L3 edge XANES spectrum of a packed powder bed containing 0.94 wt % Pt/Al_2O_3. The absolute edge-step is indicated in blue. (b) Calibration curves for different Pt loadings of Pt/Al_2O_3 and Pt/CeO_2 packed powder beds. The dashed red lines are linear fits of the data points. The linear dependency between Pt loading and edge-step allows the determination of the Pt loading during experiments. (c) Theoretical progression of the number of photons with an energy of 11564 eV (Pt L3-edge) for different penetration depths inside of CeO_2 and Al_2O_3 particles. Calculations were conducted with the Hephaestus software.[26] Changes due to the presence of pores were neglected for these calculations.

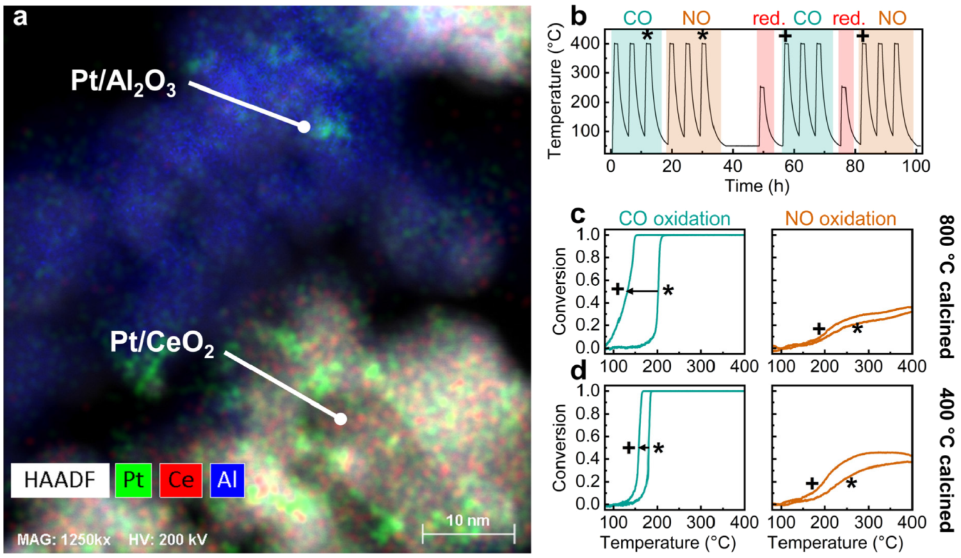

Figure 3. (a) EDX analysis of a mixed powder bed consisting of 1.9 wt % Pt/Al_2O_3 and CeO_2 after 12 h of calcination at 800 °C in static air followed by a reduction step. (b) Experimental procedure for both catalysts after 12 h of calcination in static air at 800 and 400 °C, respectively: CO oxidation (blue) and NO oxidation (orange) light-off with reduction steps (red) in between. The light-offs used for discussion are marked with symbols (*, +). (c, d) CO oxidation (blue) and NO oxidation (orange) light-off curves for the two catalysts.

order = 3) lines were determined using the Athena software.[26] With increasing fractions of Pt, the absorption and therefore also the fluorescence signal increase linearly. In Figure 2b, the measured ratios of the Pt loading and the edge-step are shown for Pt/Al_2O_3 and Pt/CeO_2. Each measurement point in this figure was obtained from the edge-step of a packed powder bed with a different Pt loading. These Pt loadings were obtained by dilution of the catalyst with the respective support material. For all these measurements, the distance and angle of the fluorescence detector were held constant since the fluorescence intensity decreases over distance and varies with the angle.[27] From the edge-step, the Pt mass (m_{Pt}) can be determined under the assumption that the loading is constant for the respective half of the catalyst bed. As an example, the 1.9 wt % Pt/Al_2O_3 powder bed mass was 1.9 mg. This resulted in a Pt mass of $m_{\mathrm{Pt,Al2O3start}} = \mathrm{Pt\ loading} \times \frac{1.9\ \mathrm{mg}}{2}$ for the first half of the 1.9 wt % Pt/Al_2O_3 packed powder bed.

For the Pt on Al_2O_3 bed, the Pt loading at $t = 0$ h was determined to be 1.77 and 1.26 wt % for the start and end positions, respectively. Since the catalyst is known to exhibit 1.9 wt % of Pt, it is likely that the amount of sample probed by the X-ray beam was not identical to that of the calibration experiments (Figure 2). For the determination of the calibration curves, packed powder beds much longer than the beam size were utilized. For the migration experiment, the catalyst beds were shorter (around 3 mm in length). Therefore, it is possible that the beam which hits the catalyst surface under an angle of about 45° did not probe the whole sample (see SI for sketch). For the CeO_2 bed, such errors can be excluded due to the strong absorption of CeO_2 which allows only the detection of fluorescence from near the surface. Because the Pt loading was shown to exhibit a linear dependency on the edge-step, the calculated Pt loadings of Pt/Al_2O_3 were multiplied by a constant in order to adjust for the nonprobed Pt/Al_2O_3 volume.

CeO_2 is known to be highly absorbent for X-rays. Figure 2c shows that for a photon energy of 11564 eV, only about 20% of the X-rays will be able to penetrate further than 20 μm inside the 100−200 μm large CeO_2 particles. Given that the fluorescence radiation must also be able to penetrate the same thickness of CeO_2 backward in order to reach the fluorescence detector, XAS can be assumed to provide only a signal from the outer shell of the CeO_2 particles. Note that in reality the 100−200 μm large CeO_2 particles also exhibit pores, and therefore X-rays will in average be able to penetrate deeper than Figure 2c suggests. Such pores can potentially cause problems for the quantification of Pt on CeO_2 during the migration experiment. Potentially limited gas phase transport of PtO_2 into the pores can impact the Pt distribution throughout the depth of the CeO_2 particles. Since, for CeO_2, not the whole particle is probed due to the strong absorption of the X-rays, the amount of Pt determined by a comparison to the calibration displayed in Figure 2b can consequentially be distorted. There is, however, no method for determining if the transport was subject to mass-transfer limitations during the Pt migration in O_2 due to the lack of the reaction rate, which would be needed in order to compare it to the pore diffusion. Because PtO_2 which is formed may adsorb, dissociate, and be formed again throughout the Pt/Al_2O_3 and the CeO_2 beds and only the total amount of Pt is tracked at 4 different positions, no reaction rate can be estimated.

Density Functional Theory Calculations

The Vienna Ab Initio Simulation Package (VASP) was used to model Pt single atom systems on different surfaces of CeO_2.[28,29] A plane-wave basis set with a cutoff energy of 450 eV, the projector augmented wave method (PAW),[30,31] and the Bayesian Error Estimation Functional with van der Waals correlations (BEEF-vdW)[32,33] exchange−correlation functional were utilized. For a better description of the delocalized Ce f orbitals, the applied GGA + U (U = 5.0 eV) method was applied.[34] The infinite slab models, used to represent different facets of CeO_2, consisted of three (110) or four (111), (211), and (221) layers thick 2 × 2 × 1 unit cells, separated by more than 15 Å of vacuum in the z direction. Atoms in the top two layers were allowed to relax during geometry optimizations. The Brillouin zones were sampled using a (4 × 4 × 1) Monkhorst−Pack k-point grid[35] for (111) and (110) facets, (6 × 6 × 1) for (100), and (3 × 4 × 1) for (221) and (211) surfaces. The convergence criterion for geometry optimizations was a maximum force of 0.01 eV per Å. Spin polarization was considered in all of the calculations.

■ RESULTS AND DISCUSSION

Pt Migration on the Molecular and Grain Size Level from Pt/Al_2O_3 to Adjacent CeO_2

In order to investigate the migration of Pt on a sub μm length scale, migration experiments were carried out on mixed powders containing 1.9 wt % Pt/Al_2O_3 and CeO_2 powder in a mass ratio of 1:1. The powders were calcined for 12 h in static air at different temperatures, namely 400 °C and 800 °C. Subsequent to the calcination, lean CO and NO oxidation light-offs with reductive pretreatments were conducted. Hereby, the aim was to uncover the impact of migration on the catalytic activity of highly dispersed and larger, reduced particles. The energy-dispersive X-ray spectroscopy (EDX) map displayed in Figure 3a shows the distribution of Pt (green), Al (blue), and Ce (red) in the catalyst after 12 h of migration at 800 °C. Pt was found on Al_2O_3 and CeO_2, confirming the migration of Pt within the nm−μm length scale in agreement with the literature.[7,19] However, no Pt was found on CeO_2 in the case of calcination at 400 °C (see TEM in SI). This is in line with the literature, where the migration of Pt in the form of PtO_2 has been shown[6] and calculated[7] to have little impact at 400 °C under oxidative conditions. Furthermore, a single Pt/Al_2O_3 particle with a diameter of about 10 μm within an environmental cell was investigated in synthetic air. The X-ray fluorescence intensity of the Pt-Lβ fluorescence line originating from the investigated particle decreased over time, indicating that Pt becomes mobile under oxidizing conditions. More details can be found in Chapter "*In situ* fluorescence study of a Pt/Al_2O_3 particle" in the SI.

In addition, a series of lean CO and NO oxidation light-offs were conducted (Figure 3b) to investigate the aging effect on the activities, which are highly dependent on the Pt particle size and its support material. Light-offs were always performed 3 times in succession in order to ensure reproducibility, and after each CO and NO oxidation light-off series, a reduction step was introduced to increase the Pt particle size. Note that 2 reduction steps were conducted due to an expected redispersion of Pt on CeO_2 during lean CO oxidation at 400 °C.[24,36] The impact of the reduction step on catalytic activity was obtained by comparison of the last CO and NO oxidation light-offs before reduction and the first CO and NO light-offs after reduction. The first two light-offs before the reduction steps were used to clean the surface. The respective second and third light-offs after reduction may differ from the first light-off after reduction due to Pt redispersion on CeO_2 for the sample calcined at 800 °C, which is the reason why they were not used for the comparison of the catalytic activity (all light-off curves are displayed within the SI).

The direct comparison of the CO oxidation light-offs (Figure 3c, d left, *) revealed that the light-off temperature $T_{50\%}$ of the catalyst calcined at 800 °C was 22 K higher than that of the catalyst calcined at 400 °C. This catalytic behavior fits well with the migration of Pt to the CeO_2 support. During the calcination at 800 °C, the formation of Pt single atoms on CeO_2 occurs *via* atom trapping.[19] As such, Pt single atoms on CeO_2 are known to be less active than Pt particles on Al_2O_3,[24,37] and the CO oxidation activity of the catalyst calcined at 800 °C was accordingly lower than that of the one calcined at 400 °C. After the reduction step, the CO oxidation activity improved for both catalysts (Figure 3c and d, left, +). However, the catalyst calcined at 800 °C with the proven migration of Pt showed a stronger activity improvement. By the reductive treatment, $T_{50\%}$ could be decreased by 150 K. In contrast to that, the catalyst calcined at 400 °C where Pt was located on Al_2O_3 showed only a decrease in $T_{50\%}$ by 60 K. It has been reported[36] that the reduction at temperatures as low as 250 °C leads to the formation of Pt clusters on CeO_2, which are more effective for CO oxidation.[38] The strong interaction with CeO_2 in contrast to Al_2O_3 enables a Mars−van Krevelen-like mechanism for Pt/CeO_2[39,40] and, by this, increases the observed CO oxidation rates for Pt particles which are only a few nanometers in size significantly in the low-temperature regime. In the case of the NO oxidation reaction (Figure 3c, d right), both catalysts showed NO conversion below 50% within the experimental temperature range. The catalyst without migrated Pt was slightly more active, displaying 37% NO conversion at 400 °C (Figure 3d, right, *), while the catalyst which experienced migration displayed only 32% NO conversion at 400 °C (Figure 3c, right, *). The higher activity might be explained by the lower efficiency of Pt single atoms on CeO_2 for NO oxidation in contrast to that of Pt particles on Al_2O_3. The generally lower activity for highly dispersed Pt on CeO_2 for the NO oxidation reaction is caused by the high oxidation state of small Pt particles in general.[41] NO conversion increased for both catalysts after the reduction step. According to the literature, the increase in the catalytic activity can be linked to the increase in the Pt particle size on Al_2O_3.[41] The reduction steps (Figure 3c and d, right, +) lowered $T_{25\%\ \mathrm{NO}}$ conversion for the catalyst calcined at 400 °C by 50 K and for that calcined at 800 °C even by 75 K. However, NO conversion was still superior for the catalyst calcined at 400 °C (43% NO conversion) in contrast to the catalyst calcined at 800 °C (36% NO conversion). This suggests that, while the increase in activity was more pronounced for Pt on CeO_2, the Pt particles on the CeO_2 support were still not the right size to outperform Pt/Al_2O_3.

Within this section, the migration of Pt from Al_2O_3 to adjacent CeO_2 particles was observed on the nm to μm length scale for 12 h of calcination in static air at 800 °C. Such a Pt migration was not observed during calcination at 400 °C, resulting in vast differences between the catalytic activities of the samples calcined at these temperatures.

Pt Migration on the Millimeter Scale from Pt/Al_2O_3 to CeO_2

After the migration of Pt has been shown to occur under oxidative conditions at 800 °C within the nm−μm regime, the migration on the mm scale is investigated in the next step. For this purpose, the method depicted in Figure 2 for *in situ* tracking the catalyst Pt content in a time and spatially resolved manner was used.

For the space- and time-resolved quantification of the catalyst's Pt content, *in situ* XAS measurements were conducted at two positions of the Pt/Al_2O_3 and CeO_2 bed, respectively (cf. Figure 1b). As depicted in Figure 4a, the spatially separated 1.9 wt % Pt/Al_2O_3 and CeO_2 packed powder beds were first exposed to a lean CO oxidation reaction mixture (1000 ppm of CO, 10% O_2 and He) for increasing temperatures in order to obtain the initial CO light-off temperature of the dual bed. This treatment was followed by 16 h of gas phase migration at a maximum temperature of approximately 800 °C under oxidative conditions (10% O_2 and He). During the 16 h of migration, the Pt loading of the first and second halves of the Pt/Al_2O_3 and CeO_2 powder bed was monitored *via in situ* XAS. Afterward, a second CO oxidation light-off was performed in order to compare the light-off temperatures before and after the Pt migration. The temporal evolution of Pt loadings and Pt mass (m_{Pt}) during the oxidative treatment at the 4 positions of the two catalyst beds (labeled as "start" and "end" in Figure 1b) is depicted in Figure 4d and e. During the migration at T_{max} = 800 °C ($T_{average} \approx$ 670 °C), the Pt loading decreased over time at the start and end of the Al_2O_3 bed in a linear manner. Within 16 h, the total Pt loss of the Pt/Al_2O_3 catalyst was about 13% (Figure 4d). On the CeO_2 powder bed catalyst (Figure 4e), the amount of Pt at the start position increased strongly within the first 4 h, then increased only slightly, and reached a steady state after 10 h. For the end position, no gain in Pt occurred within the first 4 h, followed by a linear increase in Pt loading. The observed migration of Pt had an impact on its CO oxidation activity.

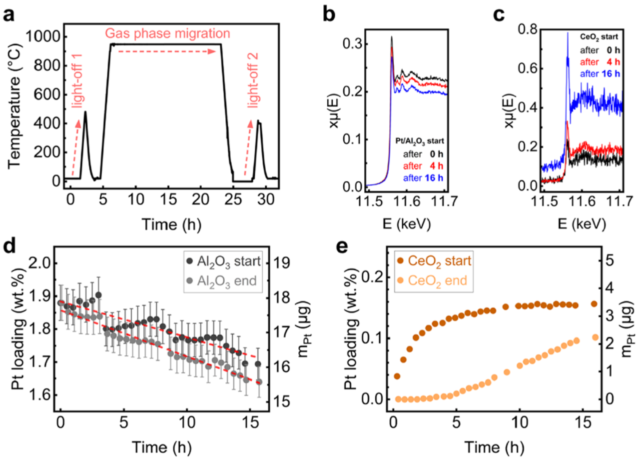

Figure 4. (a) Experimental procedure: Lean CO oxidation light-off was followed by oxidative treatment and finalized with a second CO oxidation light-off. All displayed temperatures are those of the gas blower. (b, c) Time-dependent, non-normalized XANES evolution of the start positions of the Pt/Al_2O_3 and the CeO_2 packed powder beds during the migration. (d, e) Time evolution of the Pt loading (also displayed as the amount of Pt) for two positions on the Al_2O_3 and CeO_2 powder beds. The dashed red lines in (d) are linear fits.

Figure 5a displays the CO conversion rate during the light-offs. The light-off temperature $T_{50\%}$ increased from before to after the Pt migration by 100 K, which might be due to the growth of Pt particles on Al_2O_3 above their optimal size of 2−3 nm for lean CO oxidation[41−43] or as discussed before due to the dispersion of migrated Pt on CeO_2[36] known to exhibit only little CO oxidation activity.[24] For a deeper understanding of the significant change in CO oxidation light-off temperature, time-resolved *operando* XANES were measured during the light-offs. The chemical Pt state, recorded at the start position of the Al_2O_3 bed during the CO oxidation light-off, displayed a typical behavior of slight reduction followed by reoxidation when CO is being converted (Figure 5b).[40,44] Pt on CeO_2 showed the same behavior (Figure 5c) after the migration as Pt/Al_2O_3 did before migration. However, there was one difference. While the normalized XANES of Pt on Al_2O_3 exhibited a white line intensity of $x\mu$ = 1.73 at room temperature, that of Pt on CeO_2 was $x\mu$ = 2.63. Note that the white line intensity increases with the oxidation state. A higher white line intensity is typical for oxidized, highly dispersed species due to their large surface to volume ratio. With increasing particle size, particles become increasingly reduced even if their surface is oxidized due to the bulk sensitivity of XAS. The 13% of Pt transfer from Al_2O_3 to CeO_2 cannot account for a $T_{50\%}$ increase of 100 K, independent of the catalytic activity of Pt/CeO_2. Thus, the lower CO conversion in Figure 5a after the migration has to at least partly be attributed to growth in the Pt particle size on Al_2O_3.

In this section, Pt migration has been observed *in situ* in a time and spatially resolved manner on the mm length scale. Furthermore, the impact of the migration of Pt from Pt/Al_2O_3 to CeO_2 on the catalytic activity was discussed. Interestingly, for the CeO_2 bed (Figure 4e), a nonlinear trend in the time-

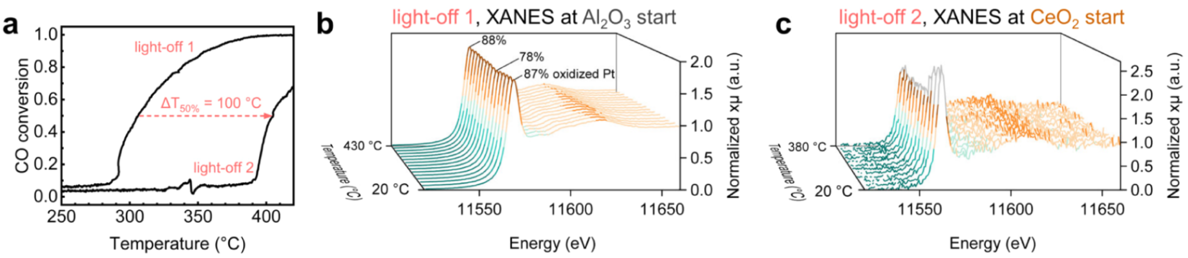

Figure 5. (a) CO conversion rate against gas blower temperature during the lean CO oxidation light-offs. (b, c) Pt L3-edge fluorescence XANES evolution during the light-offs recorded at the start position of Al_2O_3 before migration and the start position of CeO_2 after migration. The fractions of oxidized Pt obtained by LCA with reduced and oxidized Pt references are depicted in (b). For (c), LCA was not conducted because XANES alignment was not possible due to the strong X-ray absorbing nature of CeO_2.

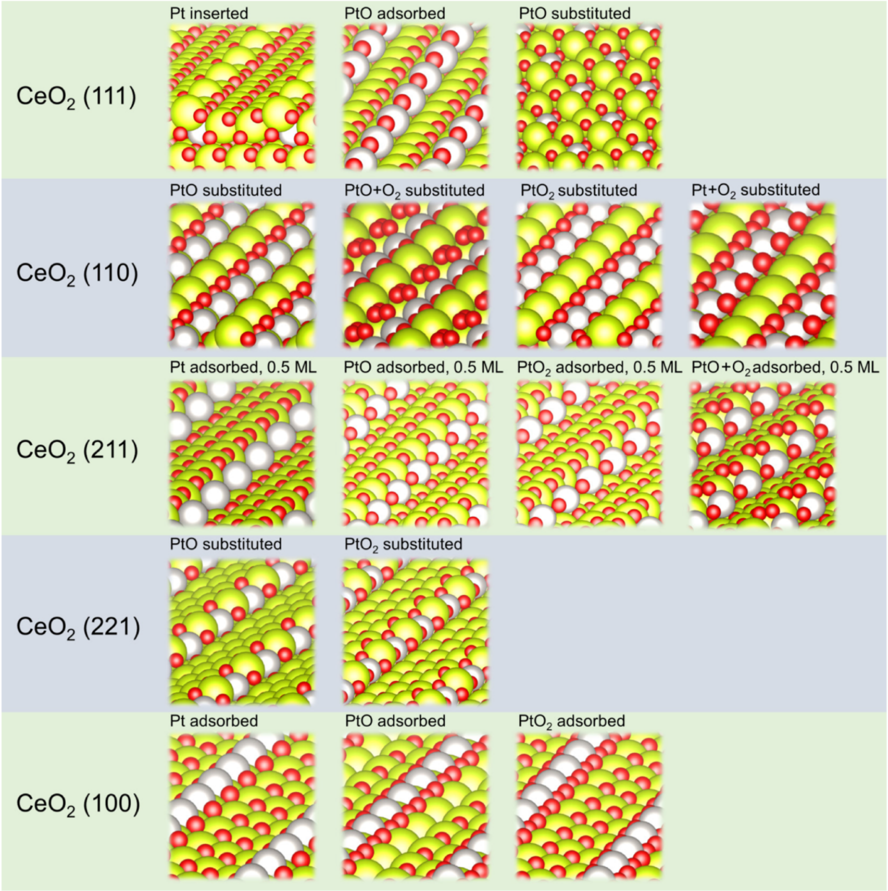

Figure 6. DFT models for Pt inserted/adsorbed and substituted on CeO_2 (111), (110), (211), (221), and (100). These structures were visualized using the Vesta software.[46]

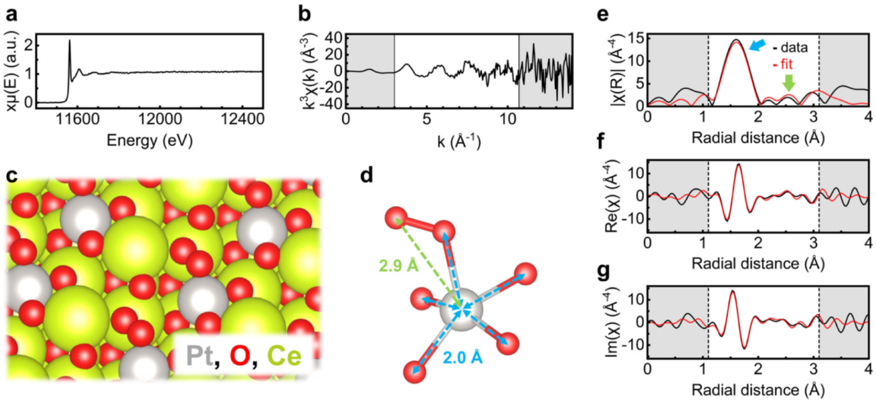

Figure 7. XAS data (Pt L3-edge) and EXAFS evaluation of CeO_2 after 16 h of migration. a) Merged and normalized X-ray absorption spectrum consisting of the CeO_2 start and end positions (positions 3 and 4) measured under oxidizing conditions at room temperature after the 16 h of migration. b) k^3 weighted $\chi(k)$ of the merged XAS scan. c) DFT-calculated atomic model of Pt incorporated into 4 fold hollow sites of the CeO_2 (110) facet with O_2 for stabilization, which yielded the best results for the EXAFS evaluation. It is labeled in Figure 6 as "CeO_2 (110) PtO + O_2 substituted". d) Closest oxygen atoms to the average Pt atom. The blue and green arrows display the distance between Pt and O. (e, f) k^3 weighted χ as well as the EXAFS fit with the structure depicted in c) are displayed in the absolute $|\chi|$, the real space Re(χ), and the imaginary space Im(χ) against the radial distance (not phase shift corrected). For b), e), f), and g), the areas with white background display the data range used for fitting.

dependent increase in Pt loading was observed. The saturation of the first half of the CeO_2 bed at a Pt loading of only 0.16 wt % is lower than reported in the literature, where weight loadings up to 3 wt % of Pt single atoms on CeO_2 have been reported. This raises the question if Pt atoms can, under these conditions, only be deposited on certain CeO_2 sites.[45] Furthermore, as this study shows, it is important to consider intra- and interparticle migration.

CeO_2 Sites for Trapping Gaseous PtO_2

In order to understand the origin of an upper Pt loading on CeO_2 (Figure 4e), the number of surface sites available for Pt adsorption is estimated. If all possible adsorption sites for Pt on the CeO_2 start position are fully occupied, then gaseous PtO_2 would be forced to move further downstream of the catalyst bed before adsorbing.

To identify how the migrated PtO_2 is present on CeO_2, XAS spectra were recorded at the start and end positions of the CeO_2 bed (at room temperature after 16 h of migration). The spectra of both positions were merged and smoothed afterward because of the low signal-to-noise ratio resulting from the low Pt loading. Various structural models obtained from density functional theory (DFT) calculations were considered for fitting the experimental EXAFS data (Figure 6).

Because of the low Pt loading and its exposure to oxidizing conditions at high temperatures, the Pt is expected to be present as oxidized Pt single atoms in accordance with the literature.[36,45] PtO species adsorbed on CeO_2(211) or substituted into CeO_2(111) and CeO_2(110) facets with a 4-fold planar geometry were found in the literature to exhibit the best stability.[24] Therefore, the considered DFT models featured Pt atoms on CeO_2 (211), (111), and (110) facets. Furthermore, other facets, namely (221) and (100), were also considered. Figure 6 displays these DFT models for single Pt atoms on CeO_2. Figure 7c displays the DFT model, which resulted in the best EXAFS fit. This specific structure has also been reported in literature.[47]

The structural model displayed in Figure 7c was the only one out of the models depicted in Figure 6 that resulted in an appropriate fit of the EXAFS data. It exhibits a geometry where Pt is surrounded by four oxygen atoms, and a neighboring Ce atom lacks an oxygen atom. Such a structural arrangement offers the possibility of additional molecular oxygen being stabilized at the position of the missing atomic oxygen on the Ce atom, with the other end pointing toward the Pt surface. The k^3-weighted $|\chi(R)|$ spectrum shown in Figure 7e exhibits a maximum at 1.6 Å. It originates from the backscattering of electrons at the five nearest oxygen atoms at a distance of approximately 2.0 Å (marked by blue arrows in Figure 7d). Another maximum at 2.5 Å can be accounted for by an oxygen atom of O_2 at a distance of 2.9 Å, which is marked by a green arrow in Figure 7d. The backscattering contribution at 3.0 Å in the plot can be accounted for by single scattering of the electrons on Ce atoms at distances between 3.2 and 3.3 Å. Note that apart from the EXAFS fit, the DFT calculations also indicate that Pt substitution in the CeO_2 (110) facet is more favorable by 1.560 eV at 1/4 monolayer coverage. CeO_2 (110) is hence stabilized by -0.030 eV/Å^2 upon Pt substitution in comparison to the substitution on CeO_2 (111), an effect that is of the same magnitude as the preferential surface energy of clean CeO_2 (111) over CeO_2 (110) of -0.032 eV/Å^2. We thus speculate that the observation of the CeO_2 (110) facet in our catalyst is due to Pt-induced surface segregation as Pt significantly stabilizes the CeO_2 (110) facet over CeO_2 (111). Details are provided in the Supporting Information.

Based on the structural model optimized by DFT calculations depicted in Figure 7c, the theoretical coverage of the CeO_2 bed start position (Figure 4e, start) was estimated. After 16 h of high temperature Pt migration under oxidative conditions, the first half of the CeO_2 bed (Figure 4e, start) contained 3.45 μg of Pt, which corresponds to 1.1×10^{16} Pt atoms. BET measurements conducted separately on two identical CeO_2 catalyst powders which were calcined for 5 h at 800 and 700 °C revealed a specific CeO_2 surface area of 73 and 104 $\frac{m^2}{g}$, respectively. These calcination temperatures were chosen because they were close to the temperature during the migration experiment. From these BET surfaces and the mass of the CeO_2 beds, first half (2.2 mg), the total area of the CeO_2 start position was estimated to be around 0.16 up to 0.23 m^2. In the DFT calculated model, each surface area of 42.52 Å^2 contains one Pt atom. The surface therefore provides space for 3.8×10^{17} up to 5.4×10^{17} Pt atoms. The experimental data in combination with the DFT model result in a surface Pt coverage of 2−3%. This estimated coverage is too low to explain the observed steady state of the CeO_2 start position. While there is a strong gradient along the axial direction of the CeO_2 bed (Figure 4e), the occurrence of gradients inside the grains cannot be excluded. Since the calibration (Figure 2b) was conducted on powders with homogeneous Pt distributions inside the grains, such gradients are a potential source of error in the determination of the Pt content. In order to trap Pt on the CeO_2 surface, the exposed surface facets play a crucial role. CeO_2 is known to exhibit multiple facets.[48] The fraction of the (111) facet in particular, which is the thermodynamically most stable CeO_2 facet, is known to increase with temperature under oxidative conditions.[49] While gaseous Pt has been claimed to adsorb near Ce^{3+} sites and edge-steps on CeO_2 (111) surface facets,[45] our experiments could be best represented by Pt in hollow sites on the (110) CeO_2 facet, as shown by the EXAFS evaluation (Figure 7). Since this facet only makes up a part of the total CeO_2 surface, the (110) surface saturation with Pt exceeds the calculated 2−3% of coverage. For a CeO_2 surface facet ratio of (110)/others ≈ 1/40, the CeO_2 (110) surface coverage with Pt would reach 100%, and the observed steady state in the Pt content of the CeO_2 start position in Figure 4e could be explained.

■ CONCLUSIONS

In this work, the migration of Pt from Al_2O_3 to CeO_2 was investigated on multiple length scales ranging from the nm scale using TEM over the μm scale using X-ray fluorescence up to the mm scale using XAS. In a first experiment, a Pt/Al_2O_3 and a CeO_2 powder were mixed and calcined in air at 400 and 800 °C, respectively. *Via* TEM, the migration of Pt onto CeO_2 was revealed to take place on the molecular and grain size scale for calcination at 800 °C but not at 400 °C. The CO and NO oxidation reactions were utilized to investigate the impact of the Pt migration on the conversion. Here, migration was shown to have a positive impact on the CO oxidation reaction and a negative impact on the NO oxidation reaction. However, an additional reaction step after the light-offs revealed a stronger improvement in activity for both reactions for the mixed powder that experienced Pt migration. This might be explained by the particle size dependencies of the activities on both support materials. Furthermore, the migration was tracked on the μm scale by X-ray microscopy, revealing a significant loss in Pt content for a 10 μm large Pt/Al_2O_3 particle within several hours. On the mm scale, the Pt migration was observed for a spatially separated dual bed by *in situ* XAS in a time and spatially resolved manner. The absolute values of the XAS edge-steps were used to quantify the Pt loading of Pt/Al_2O_3 and Pt/CeO_2 catalysts. At a maximum temperature of 800 °C under oxidative conditions, Pt migrated from a 1.9 wt % Pt/Al_2O_3 powder bed to a CeO_2 bed, which was spatially separated by a distance of roughly one millimeter. Within 16 h, 13% of the Pt migrated from the 1.9 wt % Pt/Al_2O_3 catalyst bed to a fixed bed of high surface area CeO_2. The migrated Pt atoms were identified by EXAFS together with DFT-derived structural models to be present foremost on the (110) facets of the CeO_2. There, the Pt atoms were revealed to be situated in 4-fold coordinated CeO_2 hollow sites with bimolecular oxygen for stabilization. The measured Pt uptake of CeO_2 did not exceed a Pt/CeO_2 weight loading of 0.16 wt % within 16 h of migration. This limit likely originates from the reached adsorption capacity of the locally available CeO_2 sites. Macroscopic effects like a Pt distribution throughout the intraparticle pores could further add to the relatively low Pt/CeO_2 loading obtained in this work. Here, spectrotomography measurements could provide the means to reveal the Pt single site distribution throughout the pores of CeO_2. Furthermore, it would be of interest to vary the surface area of CeO_2 and the grain size of the CeO_2 powder. The presented XAS-based method for tracking the Pt loading can be used as an experimental tool for *in situ* and *operando* studies on high temperature reactions as well as for the generation of Pt-based single-site catalysts. Furthermore, knowledge about the preferential Pt adsorption sites can be used to create spatial gradients during the synthesis of Pt-based single-site catalysts.

■ ASSOCIATED CONTENT

Data Availability Statement

The data is available at KIT open under the following link: https://doi.org/10.35097/nw11yua6ek6t2nbf

Supporting Information

The Supporting Information is available free of charge at https://pubs.acs.org/doi/10.1021/acs.jpcc.5c05574.

> Additional information on CO and NO oxidation light-offs as well as HAADF-STEM, XAS, EXAFS, and XRF and DFT structures (PDF)

■ AUTHOR INFORMATION

Corresponding Authors

Yolita M. Eggeler − *Laboratory for Electron Microscopy (LEM), Karlsruhe Institute of Technology (KIT), Karlsruhe 76131, Germany*; Email: yolita.eggeler@kit.edu

Jan-Dierk Grunwaldt − *Laboratory for Electron Microscopy (LEM), Karlsruhe Institute of Technology (KIT), Karlsruhe 76131, Germany; Institute of Catalysis Research and Technology (IKFT), Karlsruher Institute of Technology (KIT), Karlsruhe, Eggenstein-Leopoldshafen 76344, Germany*; orcid.org/0000-0003-3606-0956; Email: grunwaldt@kit.edu

Authors

Samuel Struzek − *Institute for Chemical Technology and Polymer Chemistry (ITCP), Karlsruhe Institute of Technology (KIT), Karlsruhe 76131, Germany*

Birger Holtermann − *Laboratory for Electron Microscopy (LEM), Karlsruhe Institute of Technology (KIT), Karlsruhe 76131, Germany*

Shweta Sharma − *Institute for Chemical Technology and Polymer Chemistry (ITCP), Karlsruhe Institute of Technology (KIT), Karlsruhe 76131, Germany*; orcid.org/0000-0002-0355-176X

Florian Maurer − *Institute for Chemical Technology and Polymer Chemistry (ITCP), Karlsruhe Institute of Technology (KIT), Karlsruhe 76131, Germany*; orcid.org/0000-0002-3307-4132

Jelena Jelic − *Institute of Catalysis Research and Technology (IKFT), Karlsruher Institute of Technology (KIT), Karlsruhe, Eggenstein-Leopoldshafen 76344, Germany*; orcid.org/0000-0002-2701-0765

Anna Zimina − *Institute of Catalysis Research and Technology (IKFT), Karlsruher Institute of Technology (KIT), Karlsruhe, Eggenstein-Leopoldshafen 76344, Germany; Institute for Chemical Technology and Polymer Chemistry (ITCP), Karlsruhe Institute of Technology (KIT), Karlsruhe 76131, Germany*; orcid.org/0000-0002-3111-7741

Felix Studt − *Institute for Chemical Technology and Polymer Chemistry (ITCP), Karlsruhe Institute of Technology (KIT), Karlsruhe 76131, Germany; Institute of Catalysis Research and Technology (IKFT), Karlsruher Institute of Technology (KIT), Karlsruhe, Eggenstein-Leopoldshafen 76344, Germany*; orcid.org/0000-0001-6841-4232

Complete contact information is available at: https://pubs.acs.org/10.1021/acs.jpcc.5c05574

Notes

The authors declare no competing financial interest.

■ ACKNOWLEDGMENTS

This study was funded by the Deutsche Forschungsgemeinschaft (DFG, German Research Foundation)—SFB 1441—Project-ID 426888090. The authors want to thank Joachim Czechowsky (ITCP, KIT) for providing the catalysts for the *in situ* experiments and for performing the XRD and BET measurements, as well as Dr. Deniz Zengel for the preparation of the mixed $Pt/Al_2O_3 + CeO_2$ catalysts for the catalytic *ex-situ* measurements and TEM investigations. The authors want to thank Carina B. Maliakkal (Institute of Nanotechnology, KIT) for the TEM analysis of the initial Pt particle sizes of the Pt/Al_2O_3 and Pt/CeO_2 catalysts and Dr. Thomas Bergfeldt (Institute of Applied Materials Science, KIT) for the ICP-OES analysis of the catalysts. Furthermore, the authors acknowledge the Deutsches Elektronen-Synchrotron (DESY), a member of the Helmholtz Association HGF, for beamtime at the P65 (Project ID: I-20220469) and P06 (Project ID: I-20231283) beamlines and the ErUM-Pro program of the German Federal Ministry of Education and Research (BMBF) for supporting the infrastructure at DESY. Additionally, the authors acknowledge E. Welter, Regina Biller, and D. B. Brueckner for their kind assistance during the beamtimes, as well as Dr. Martin Peterlechner for the fruitful discussion regarding EDX analysis and quantification. They also thank Dr. Torsten Scherer (Institute of Nanotechnology, KIT) for his help with the sample preparation by FIB for the XRF measurements. Furthermore, the authors thank Tim Delrieux (ITCP, KIT), Leonardo De Campos (ITCP, KIT), and Dr. Thomas Sheppard (TU Wien) for joining beamtime. Dr. Jelena Jelic and Dr. Felix Studt acknowledge support from the state of Baden-Württemberg through bwHPC and the German Research Foundation (DFG) through grant no. INST40/575-1FUGG (JUSTUS2 cluster, RVs bw17D011). Support from the Helmholtz Association is also gratefully acknowledged. Finally, the authors acknowledge DAPHNE4NFDI (DFG project under project number 460248799) as well as NFDI-consortia (NFDI4Cat, FAIRMAT, and NFDI4Chem) for fruitful discussion and valuable input for implementing FAIR data principles in this work.

■ REFERENCES

(1) Miyoshi, N.; Matsumoto, S.; Katoh, K.; Tanaka, T.; Harada, J.; Takahashi, N.; Yokota, K.; Sugiura, M.; Kasahara, K. Development of new concept three-way catalyst for automotive lean-burn engines. *SAE Trans.* **1995**, 1361−1370.

(2) Golunski, S. E.; Hatcher, H. A.; Rajaram, R. R.; Truex, T. J. Origins of low-temperature three-way activity in Pt/CeO_2. *Appl. Catal. B: Environ.* **1995**, *5*, 367−376.

(3) Gänzler, A. M.; Casapu, M.; Maurer, F.; Störmer, H.; Gerthsen, D.; Ferre, G.; Vernoux, P.; Bornmann, B.; Frahm, R.; Murzin, V.; et al. Tuning the Pt/CeO_2 interface by in situ variation of the Pt particle size. *ACS Catal.* **2018**, *8*, 4800−4811.

(4) Corro, G. Sulfur impact on diesel emission control - A review. *React. Kinet. Catal. Lett.* **2002**, *75*, 89−106.

(5) Harris, P. Growth and structure of supported metal catalyst particles. *Int. Mater. Rev.* **1995**, *40*, 97−115.

(6) Porsgaard, S.; Merte, L. R.; Ono, L. K.; Behafarid, F.; Matos, J.; Helveg, S.; Salmeron, M.; Roldan Cuenya, B.; Besenbacher, F. Stability of platinum nanoparticles supported on SiO_2/Si (111): A high-pressure X-ray photoelectron spectroscopy study. *ACS Nano* **2012**, *6*, 10743−10749.

(7) Plessow, P. N.; Abild-Pedersen, F. Sintering of Pt nanoparticles via volatile PtO_2: simulation and comparison with experiments. *ACS Catal* **2016**, *6*, 7098−7108.

(8) Alcock, C.; Hooper, G. Thermodynamics of the gaseous oxides of the platinum-group metals. *Proc. R. Soc. London A Math. Phys. Sci.* **1960**, *254*, 551−561.

(9) Schäfer, H.; Tebben, A. Gleichgewichtsmessungen im System Platin—Sauerstoff Gasförmiges Platindioxyd. *Z. Anorg. Allg. Chem.* **1960**, *304*, 317−321.

(10) Porter, S.; Ghosh, A.; Liu, C. H.; Kunwar, D.; Thompson, C.; Alcala, R.; Dean, D. P.; Miller, J. T.; De La Riva, A.; Pham, H.; et al. Biphasic Janus particles explain self-healing in Pt−Pd diesel oxidation catalysts. *ACS Catal.* **2023**, *13*, 5456−5471.

(11) Johns, T. R.; Goeke, R. S.; Ashbacher, V.; Thüne, P. C.; Niemantsverdriet, J.; Kiefer, B.; Kim, C. H.; Balogh, M. P.; Datye, A. K. Relating adatom emission to improved durability of Pt−Pd diesel oxidation catalysts. *J. Catal.* **2015**, *328*, 151−164.

(12) Xu, Z.; Li, Y.; Lin, Y.; Zhu, T. A review of the catalysts used in the reduction of NO by CO for gas purification. *Environ. Sci. Pollut. Res.* **2020**, *27*, 6723−6748.

(13) Leistner, K.; Braga, C. G.; Kumar, A.; Kamasamudram, K.; Olsson, L. Volatilisation and subsequent deposition of platinum oxides from diesel oxidation catalysts. *Appl. Catal. B: Environ.* **2019**, *241*, 338−350.

(14) Xiong, Y.; Yamaji, K.; Kishimoto, H.; Brito, M. E.; Horita, T.; Yokokawa, H. Deposition of platinum particles at LSM/ScSZ/air three-phase boundaries using a platinum current collector. *Electrochem. Solid-State Lett.* **2009**, *12*, B31.

(15) Neri, J.; Cammarata, A.; Donazzi, A. Experimental and Model Investigation of a Solid Oxide Fuel Cell Operated Under Low Fuel Flow Rate. *J. Electrochem. Soc.* **2023**, *170*, 124506.

(16) Ghosh, A.; Pham, H.; Higgins, J.; Van Swol, F.; De La Riva, A.; Melton, M.; Kunwar, D.; Qi, G.; Oh, S. H.; Wiebenga, M.; et al. Restricting the growth of Pt nanoparticles through confinement in ordered nanoporous structures. *Appl. Catal. A: Gen.* **2020**, *607*, 117858.

(17) Carrillo, C.; Johns, T. R.; Xiong, H.; De La Riva, A.; Challa, S. R.; Goeke, R. S.; Artyushkova, K.; Li, W.; Kim, C. H.; Datye, A. K. Trapping of mobile Pt species by PdO nanoparticles under oxidizing conditions. *J. Phys. Chem. Lett.* **2014**, *5*, 2089−2093.

(18) Xiong, H.; Peterson, E.; Qi, G.; Datye, A. K. Trapping mobile Pt species by PdO in diesel oxidation catalysts: Smaller is better. *Catal. Today* **2016**, *272*, 80−86.

(19) Jones, J.; Xiong, H.; De La Riva, A. T.; Peterson, E. J.; Pham, H.; Challa, S. R.; Qi, G.; Oh, S.; Wiebenga, M. H.; Pereira Hernández, X. I.; et al. Thermally stable single-atom platinum-on-ceria catalysts via atom trapping. *Science* **2016**, *353*, 150−154.

(20) Alcala, R.; De La Riva, A.; Peterson, E. J.; Benavidez, A.; Garcia-Vargas, C. E.; Jiang, D.; Pereira-Hernández, X. I.; Brongersma, H. H.; Ter Veen, R.; Staněk, J.; et al. Atomically dispersed dopants for stabilizing ceria surface area. *Appl. Catal., B* **2021**, *284*, 119722.

(21) Bruix, A.; Neyman, K. M.; Illas, F. Adsorption, oxidation state, and diffusion of Pt atoms on the CeO_2 (111) surface. *J. Phys. Chem. C* **2010**, *114*, 14202−14207.

(22) Bruix, A.; et al. Maximum noble-metal efficiency in catalytic materials: atomically dispersed surface platinum. *Angew. Chem., Int. Ed.* **2014**, *53*, 10525−10530.

(23) Agarwal, S.; Lefferts, L.; Mojet, B. L.; Ligthart, D. M.; Hensen, E. J.; Mitchell, D. R.; Erasmus, W. J.; Anderson, B. G.; Olivier, E. J.; Neethling, J. H.; et al. Exposed surfaces on shape-controlled ceria nanoparticles revealed through AC-TEM and water−gas shift reactivity. *ChemSuschem* **2013**, *6*, 1898−1906.

(24) Maurer, F.; Jelic, J.; Wang, J.; Gänzler, A.; Dolcet, P.; Wöll, C.; Wang, Y.; Studt, F.; Casapu, M.; Grunwaldt, J.-D. Tracking the formation, fate and consequence for catalytic activity of Pt single sites on CeO_2. *Nat. Catal.* **2020**, *3*, 824−833.

(25) Welter, E.; Nemausat, R. A beamline for bulk sample x-ray absorption spectroscopy at the high brilliance storage ring PETRA III. In *AIP. Conf. Proc.*; AIP Publishing LLC, 2019.*2054*, 1, 040002

(26) Ravel, B.; Newville, M. ATHENA, ARTEMIS, HEPHAESTUS: data analysis for X-ray absorption spectroscopy using IFEFFIT. *J. Synchrotron Radiat.* **2005**, *12*, 537−541.

(27) Bunker, G. *Introduction to XAFS: a practical guide to X-ray absorption fine structure spectroscopy*, 1st ed.; Cambridge University Press: Cambridge, England, 2010.

(28) Kresse, G.; Furthmüller, J. Efficiency of ab-initio total energy calculations for metals and semiconductors using a plane-wave basis set. *Comput. Mater. Sci.* **1996**, *6*, 15−50.

(29) Kresse, G.; Furthmüller, J. Efficient iterative schemes for ab initio total-energy calculations using a plane-wave basis set. *Phys. Rev. B* **1996**, *54*, 11169.

(30) Blöchl, P. E. Projector augmented-wave method. *Phys. Rev. B* **1994**, *50*, 17953.

(31) Kresse, G.; Joubert, D. From ultrasoft pseudopotentials to the projector augmented-wave method. *Phys. Rev. B* **1999**, *59*, 1758.

(32) Mortensen, J. J.; Kaasbjerg, K.; Frederiksen, S. L.; Nørskov, J. K.; Sethna, J. P.; Jacobsen, K. W. Bayesian error estimation in density-functional theory. *Phys. Rev. Lett.* **2005**, *95*, 216401.

(33) Wellendorff, J.; Lundgaard, K. T.; Møgelhøj, A.; Petzold, V.; Landis, D. D.; Nørskov, J. K.; Bligaard, T.; Jacobsen, K. W. Density functionals for surface science: Exchange-correlation model development with Bayesian error estimation. *Phys. Rev. B - Condens. Matter Mater. Phys.* **2012**, *85*, 235149.

(34) Dudarev, S. L.; Botton, G. A.; Savrasov, S. Y.; Humphreys, C.; Sutton, A. P. Electron-energy-loss spectra and the structural stability of nickel oxide: An LSDA+ U study. *Phys. Rev. B* **1998**, *57*, 1505.

(35) Monkhorst, H. J.; Pack, J. D. Special points for Brillouin-zone integrations. *Phys. Rev. B* **1976**, *13*, 5188.

(36) Gänzler, A. M.; Casapu, M.; Vernoux, P.; Loridant, S.; Cadete Santos Aires, F. J.; Epicier, T.; Betz, B.; Hoyer, R.; Grunwaldt, J.-D. Tuning the structure of platinum particles on ceria in situ for enhancing the catalytic performance of exhaust gas catalysts. *Angew.Chem., Int. Ed.* **2017**, *56*, 13078−13082.

(37) Maurer, F.; Gänzler, A.; Lott, P.; Betz, B.; Votsmeier, M.; Loridant, S.; Vernoux, P.; Murzin, V.; Bornmann, B.; Frahm, R.; et al. Spatiotemporal investigation of the temperature and structure of a Pt/CeO_2 oxidation catalyst for CO and hydrocarbon oxidation during pulse activation. *Ind. Eng. Chem. Res.* **2021**, *60*, 6662−6675.

(38) Maurer, F.; Beck, A.; Jelic, J.; Wang, W.; Mangold, S.; Stehle, M.; Wang, D.; Dolcet, P.; Gänzler, A. M.; Kübel, C.; et al. Surface noble metal concentration on ceria as a key descriptor for efficient catalytic CO oxidation. *ACS Catal.* **2022**, *12*, 2473−2486.

(39) Cargnello, M.; Doan-Nguyen, V. V.; Gordon, T. R.; Diaz, R. E.; Stach, E. A.; Gorte, R. J.; Fornasiero, P.; Murray, C. B. Control of metal nanocrystal size reveals metal-support interface role for ceria catalysts. *Science* **2013**, *341*, 771−773.

(40) Gänzler, A. M.; Casapu, M.; Doronkin, D. E.; Maurer, F.; Lott, P.; Glatzel, P.; Votsmeier, M.; Deutschmann, O.; Grunwaldt, J.-D. Unravelling the different reaction pathways for low temperature CO oxidation on Pt/CeO_2 and Pt/Al_2O_3 by spatially resolved structure−activity correlations. *J. Phys. Chem. Lett.* **2019**, *10*, 7698−7705.

(41) Boubnov, A.; Dahl, S.; Johnson, E.; Molina, A. P.; Simonsen, S. B.; Cano, F. M.; Helveg, S.; Lemus-Yegres, L. J.; Grunwaldt, J.-D. Structure−activity relationships of Pt/Al_2O_3 catalysts for CO and NO oxidation at diesel exhaust conditions. *Appl. Catal. B: Environ.* **2012**, *126*, 315−325.

(42) Lee, J.; Jang, E. J.; Oh, D. G.; Szanyi, J.; Kwak, J. H. Morphology and size of Pt on Al_2O_3: The role of specific metal-support interactions between Pt and Al_2O_3. *J. Catal.* **2020**, *385*, 204−212.

(43) Casapu, M.; Fischer, A.; Gänzler, A. M.; Popescu, R.; Crone, M.; Gerthsen, D.; Türk, M.; Grunwaldt, J.-D. Origin of the normal and inverse hysteresis behavior during CO oxidation over Pt/Al_2O_3. *ACS Catal.* **2017**, *7*, 343−355.

(44) Struzek, S.; Delrieux, T.; Maurer, F.; Gonçalves, D. S.; Heck, S.-L.; Klag, L.; Czechowsky, J.; Zimina, A.; Grunwaldt, J.-D. Role of powders and coatings for relating catalytic activity and structure of Pt in emission control catalysis. *React. Chem. Eng.* **2025**, *10*, 1233−1243.

(45) Kunwar, D.; et al. Stabilizing high metal loadings of thermally stable platinum single atoms on an industrial catalyst support. *ACS Catal.* **2019**, *9*, 3978−3990.

(46) Momma, K.; Izumi, F. VESTA 3 for three-dimensional visualization of crystal, volumetric and morphology data. *J. Appl. Crystallogr.* **2011**, *44*, 1272−1276.

(47) Dolcet, P.; Maurer, F.; Casapu, M.; Grunwaldt, J.-D. Insights into the Structural Dynamics of Pt/CeO_2 Single-Site Catalysts during CO Oxidation. *Catalysts* **2021**, *11*, 617.

(48) Aneggi, E.; Wiater, D.; De Leitenburg, C.; Llorca, J.; Trovarelli, A. Shape-dependent activity of ceria in soot combustion. *ACS Catal.* **2014**, *4*, 172−181.

(49) Yang, C.; Capdevila-Cortada, M.; Dong, C.; Zhou, Y.; Wang, J.; Yu, X.; Nefedov, A.; Heißler, S.; López, N.; Shen, W.; Wöll, C.; Wang, Y. Surface refaceting mechanism on cubic ceria. *J. Phys. Chem. Lett.* **2020**, *11*, 7925−7931.

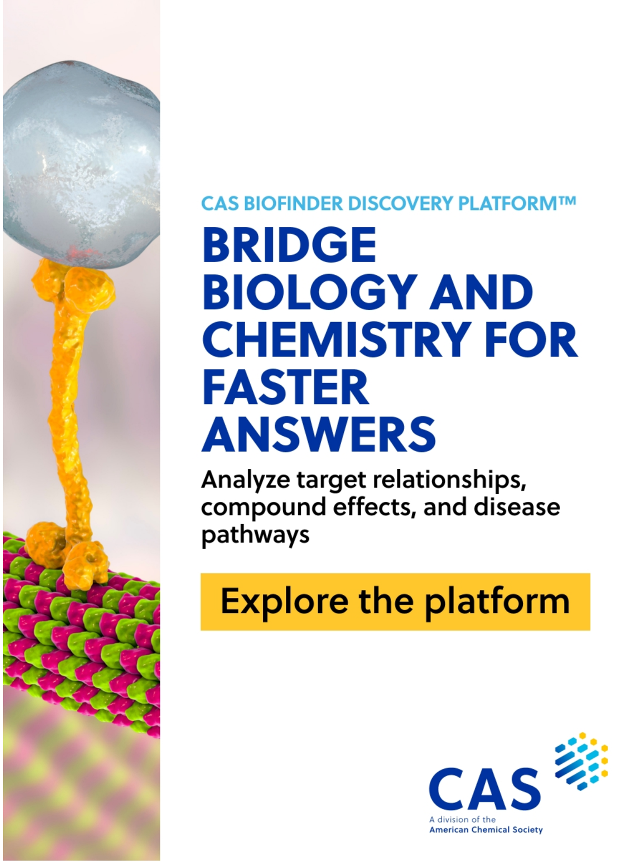

CAS BIOFINDER DISCOVERY PLATFORM™
BRIDGE BIOLOGY AND CHEMISTRY FOR FASTER ANSWERS
Analyze target relationships, compound effects, and disease pathways
Explore the platform
CAS
A division of the American Chemical Society